# Electronic and magnetic properties of a quasi-one-dimensional spin chain system $Sr_3NiRhO_6$

S. K. Pandey and Kalobaran Maiti*
*Department of Condensed Matter Physics and Materials Science, Tata Institute of Fundamental Research, Homi Bhabha Road, Colaba, Mumbai 400 005, India*

(Received 17 April 2008; revised manuscript received 7 June 2008; published 28 July 2008)

We investigate the electronic structure of $Sr_3NiRhO_6$, a quasi-one-dimensional spin chain system using *ab initio* band-structure calculations. Spin polarized calculations within generalized gradient approximation (GGA) reveal that Ni and Rh have finite moments, and they are antiferromagnetically coupled along the chain axis in the ground state. While these results that are obtained within the local spin-density approximations provide remarkable representation of the magnetic phase, the experimentally observed insulating behavior could not be captured within this method. GGA+$U$ calculations show that the opening up of an insulating gap requires on-site Coulomb interaction strength among the Rh 4$d$ electrons, $U_{dd}^{\mathrm{Rh}} \approx 2.5$ eV, and the correlation strength among Ni 3$d$ electrons, $U_{dd}^{\mathrm{Ni}} \approx 4.5$ eV, suggesting this system to be a Mott insulator. Electron correlation among $d$ electrons leads to significant enhancement of the O 2$p$ character of the energy bands in the vicinity of the Fermi level and the $d$ bands appear at lower energies. Energy gap in the up-spin density of states appears to be significantly small ($\sim$0.12 eV) while it is $>$2 eV in the down-spin density of states, suggesting a possibility of spin-polarized conduction in the semiconducting phase.

DOI: 10.1103/PhysRevB.78.045120 PACS number(s): 71.27.+a, 71.20.−b, 75.20.Hr

## I. INTRODUCTION

Recently, quasi-one-dimensional compounds, $AE_3MM'O_6$ ($AE$=alkaline earth metals such as Ca, Sr, etc.; $M$ and $M'$ are transition metals), possessing rhombohedral $K_4CdCl_6$ structure (space-group $R\bar{3}C$) have attracted a great deal of attention due to their fascinating magnetic properties.[1–16] In this structure (see Fig. 1), $MO_6$ forms in trigonal prismatic geometry and $M'O_6$ forms in octahedral geometry. These two units appear alternatively along the chain direction ($c$ axis) and are connected via face sharing, as shown in the figure. It is evident that the interchain interaction is significantly weak, making these compounds a quasi-one-dimensional system. It is observed that antiferromagnetic, ferromagnetic, or ferrimagnetic long-range ordered phases can be achieved by tuning the intrachain magnetic coupling in these one-dimension chains.[5–7] In addition to such interesting properties of the quasi-one-dimensional chains, the whole system can be viewed as made of antiferromagnetic or ferromagnetic chains arranged in a triangular lattice. Numerous studies based on tailoring the composition of these geometrically frustrated systems reveal plethora of phases such as spin-liquid phase, partially disordered antiferromagnetic phase, etc.[2–6]

In this paper, we report our results on the electronic structure of $Sr_3NiRhO_6$ using full potential linearized augmented plane-wave method. This is one of the unique compounds that exhibits antiferromagnetic intrachain coupling below 45 K, in contrast to most other compounds in this class. Further lowering in temperature leads to partially disordered antiferromagnetic phase below 10 K.[6] Interestingly, analogous compound $Sr_3NiPtO_6$ exhibits spin-liquid behavior. While it is difficult to capture disorder effect and/or spin-liquid phase using such *ab initio* band-structure calculations, $Sr_3NiRhO_6$ is a good starting point to understand the intrachain coupling and associated ground-state properties.

Our results clearly establish that the ground state of this compound consists of magnetic Ni and Rh ions, which are antiferromagnetically coupled along the $c$ axis. To capture the insulating transport that is consistent with experimental observations, one needs to consider the on-site Coulomb interaction among Ni 3$d$ and Rh 4$d$ electrons in addition to the intrachain antiferromagnetic (IAFM) coupling, which suggests that this compound is a Mott insulator. On-site Coulomb interaction among Rh 4$d$ electrons is found to be lower (about 60%) than that found for Ni 3$d$ electrons, as expected due to larger radial extension of the Rh 4$d$ orbitals.

## II. COMPUTATIONAL DETAILS

The spin-polarized generalized gradient approximation (GGA) and GGA+$U$ ($U$=on-site Coulomb repulsion strength) electronic structure calculations were carried out using *state-of-the-art* full potential linearized augmented plane-wave (FPLAPW) method.[17] The lattice parameters and atomic positions used in the calculations are taken from

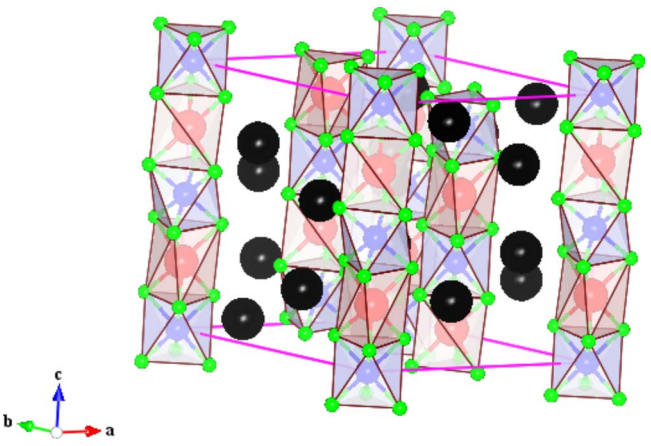


FIG. 1. (Color online) The unit cell of $Sr_3NiRhO_6$. Sr is represented by largest symbols (black). Gradually decreasing sized symbols represent Ni (pink), Rh (blue), and O (green), respectively.

 

literature.[8] The Muffin-Tin sphere radii were chosen to be 2.33, 2.19, 2.01, and 1.78 a.u. for Sr, Ni, Rh, and O atoms, respectively. For the exchange-correlation functional, we have adopted recently developed GGA form from Wu and Cohen.[18] The on-site Coulomb interactions were considered within local spin-density approximation (LSDA)+$U$ formulation of Anisimov *et al.*[19] The calculations were performed by varying on-site Coulomb interaction among Ni 3$d$ electrons, $U_{dd}^{\mathrm{Ni}}$, and Rh 4$d$ electrons, $U_{dd}^{\mathrm{Rh}}$. The convergence was achieved by considering 512 $k$ points within the first Brillouin zone and the error bar for the energy convergence was set to be smaller than $10^{-4}$ Ry/cell.

## III. RESULTS AND DISCUSSIONS

The crystal structure of $Sr_3NiRhO_6$ is hexagonal, as shown in Fig. 1, where the Sr, Ni, Rh, and O ions are denoted by spheres of decreasing size. It is evident from the figure that the Ni and Rh ions are surrounded by six oxygen ions forming trigonal prism and octahedron, respectively. The trigonal prisms and octahedra are connected by face sharing, and form the chains along the $c$ axis. *Both* Ni 3$d$ and Rh 4$d$ orbitals are not degenerate due to the corresponding crystal-field effect. The axis system is defined such that $z$ axis is along $c$ axis, and $x$ and $y$ axes are in the $ab$ plane. In this axis system, the fivefold degenerate $d$ levels will split into three energy levels consisting of $d_{z^2}$, $(d_{xz},d_{yz})$, and $(d_{x^2-y^2},d_{xy})$ orbitals. Throughout the paper, we have denoted these three bands by $d_0$, $d_{\pm 1}$, and $d_{\pm 2}$, respectively, for the sake of brevity. The energy separation and the location of the bands in the energy axis will depend on the type of crystal field applicable, as discussed later in the text.

In Fig. 2, we show the partial density of states (PDOS) corresponding to Ni 3$d$, Rh 4$d$, and O 2$p$ electronic states obtained from GGA calculations where Ni and Rh are ferromagnetically coupled. The band splitting due to the crystal field, as discussed above, is visible clearly in the figure. In Fig. 2(a), the energy range above −2 eV is essentially contributed by Ni 3$d$ electronic states. The lower energy region (−4–−2 eV) contains very low intensity of Ni 3$d$ PDOS and has dominant O 2$p$ contributions. The energy distributions of the density of states (DOS) corresponding to both Ni 3$d$ and O 2$p$ states appear similar. These results suggest that the DOS in −4–−2 eV range can be attributed to bonding states arising from Ni 3$d$ and O 2$p$ hybridizations, and the antibonding states with dominant Ni 3$d$ character appear above −2 eV.

The DOS in the energy ranges −6.3–−4.4 eV and −1.5–0 eV correspond to Rh 4$d$-O 2$p$ bonding and antibonding bands, respectively. The intensity of Rh 4$d$ PDOS is almost similar in these two regions with negligible contribution in the energy region of −4.4–−1.5 eV [see Fig. 2(b)]. Two distinct features are observed in Fig. 2. (i) The energy separation between bonding and antibonding bands arising due to Ni 3$d$-O 2$p$ hybridizations is significantly smaller than the energy separation between the bonding and antibonding Rh 4$d$-O 2$p$ bands. (ii) The bonding and antibonding Ni 3$d$-O 2$p$ bands have dominant O 2$p$ and Ni 3$d$ character, respectively. However, the mixing of Rh 4$d$ and O 2$p$ characters in the Rh 4$d$-O 2$p$ hybridization is much stronger. These observations clearly demonstrate the stronger O 2$p$-Rh 4$d$ hybridization presumably due to larger radial extension of the 4$d$ orbitals compared to the 3$d$ orbitals. Such large overlap integral $t$ leads to larger separation of the bonding and antibonding bands. However, the bandwidth of the individual bands does not appear to increase.

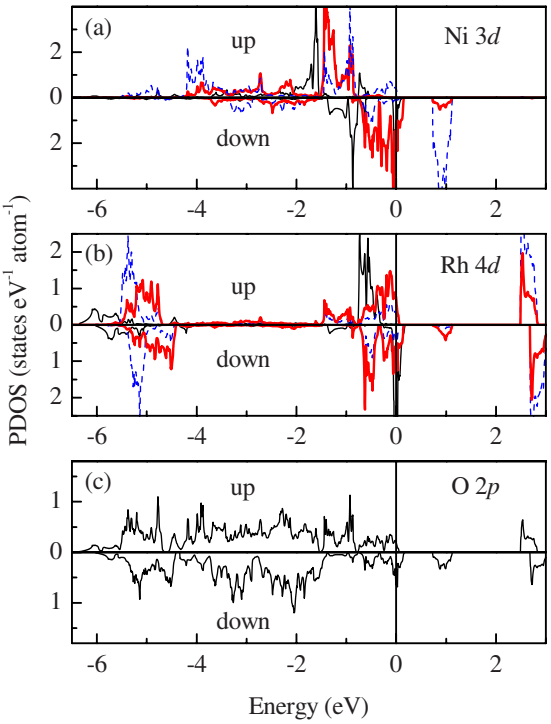


FIG. 2. (Color online) The PDOS corresponding to $d_{z^2}$ ($d_0$; thin solid lines), $d_{xz}+d_{yz}$ ($d_{\pm 1}$; dashed lines), and $d_{xy}+d_{x^2-y^2}$ ($d_{\pm 2}$; thick solid lines) orbitals for (a) Ni and (b) Rh, obtained from spin-polarized GGA calculation when Ni and Rh are ferromagnetically coupled. (c) O 2$p$ PDOS.

In addition, it is evident from Fig. 2(a) that up-spin channel of Ni 3$d$ states is almost fully occupied whereas down-spin channel is partially occupied. Major contribution in the unoccupied level comes from $d_{\pm 1}$ orbitals. In the case of Rh 4$d$ states, DOS corresponding to both the spin states are partially occupied and thus contribute to the unoccupied DOS.

The GGA calculations for ferromagnetic (FM) intrachain coupling converged to the metallic ground state in sharp contrast to the experimentally observed insulating behavior in this compound. Moreover, the total magnetic moment per formula unit (f.u.) obtained from this calculation is about $2.85\mu_B$, which is much larger than the experimentally estimated value of $\sim 1\mu_B$.[6] The magnetic moment centered at Ni and Rh sites are $1.55\mu_B$ and $0.43\mu_B$, respectively. Magnetic moment centered at the oxygen sites is found to be $0.13\mu_B$, which is large and induced by the Ni 3$d$ and Rh 4$d$ moments.

It is evident from the magnetic moments that if Ni and Rh are antiferromagnetically coupled, the total magnetic moment would match with the experimental results. In order to investigate such possibility, we have calculated the ground-state energies and wave functions corresponding to antifer-

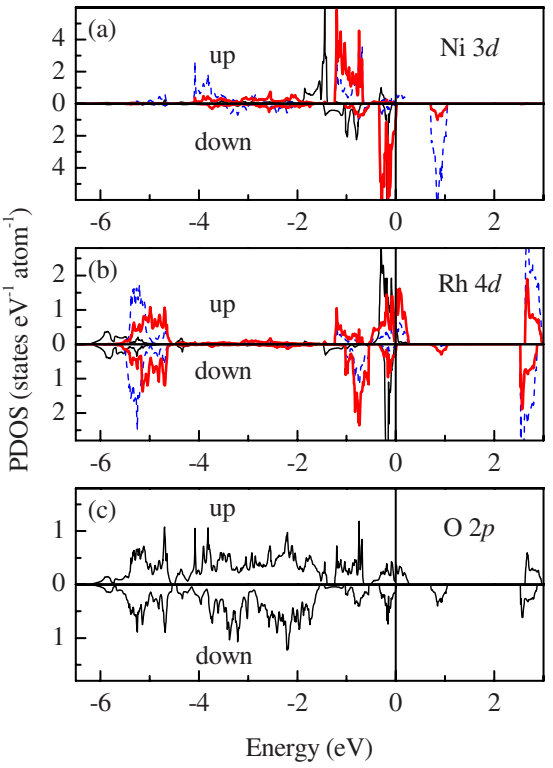


FIG. 3. (Color online) The PDOS corresponding to $d_{z^2}$ ($d_0$; thin solid lines), $d_{xz}+d_{yz}$ ($d_{\pm 1}$; dashed lines), and $d_{xy}+d_{x^2-y^2}$ ($d_{\pm 2}$; thick solid lines) orbitals for (a) Ni and (b) Rh, obtained from spin-polarized GGA calculation when intrachain Ni and Rh are antiferromagnetically coupled. (c) O $2p$ PDOS.

romagnetic coupling between Ni $3d$ and Rh $4d$ moments. Interestingly, the calculated ground-state energy is found to be 27 meV/f.u. lower than that of FM state. The calculated total magnetic moment comes out to be $1.04\mu_B$/f.u.. Both these findings provide remarkable representation of the experimental magnetization data.[6] The calculated magnetic moments for Ni and Rh are $1.31\mu_B$ and $-0.36\mu_B$, respectively. The moment centered at oxygen site is almost negligible ($0.02\mu_B$).

The calculated Ni $3d$, Rh $4d$, and O $2p$ PDOS are shown in Fig. 3. It is evident from the figure that intrachain antiferromagnetic interaction leads to significant reduction in bandwidth of all the energy bands and redistribution in spectral weight. For example, Ni $3d$ up-spin band is almost completely filled and the Fermi level $\epsilon_F$ is pinned at the top of the down-spin band, having dominant $d_{\pm 2}$ orbital contributions and a width of about 0.5 eV, while Ni $3d$ down-spin band in Fig. 2 has a width of about 1 eV and is partially filled. The occupancy of Rh $4d$ up-spin and down-spin PDOS exhibit spectral distribution opposite to that observed in Fig. 2, as expected, due to antiferromagnetic coupling. In this case also, the bands are narrower than those observed in Fig. 2. The O $2p$ contribution at the Fermi level is dominant for up spin while in the ferromagnetic case, it was down spin.

All the above results clearly establish that the LSDA approach is adequate to capture the magnetic phase in this system. Although, there is significant spectral weight redistributions observed for different magnetic configurations, both these calculations converge to metallic ground state, in contrast to the experimental studies.

It is well known that such *ab initio* calculations often underestimate the on-site Coulomb correlation energy, which plays significant role in determining the electronic properties of $d$ and $f$ electron systems.[20] The consideration of on-site Coulomb interaction among the $d$ electrons ($U_{dd}$) under GGA+$U$ formulation is expected to improve the situation. Thus, we have carried out GGA+$U$ calculations for different values of $U_{dd}$ corresponding to Ni $3d$ electrons, which is defined as $U_{dd}^{\mathrm{Ni}}$, and Rh $4d$ electrons, which is defined as $U_{dd}^{\mathrm{Rh}}$.

We have carried out GGA+$U$ calculations for $U_{dd}^{\mathrm{Rh}}=3$ eV and $U_{dd}^{\mathrm{Ni}}=5$ eV, considering both FM and IAFM couplings. The ground state is found to be insulating in both the cases. We find that the total energy for the FM state is about 62.5 meV/f.u. lower than that for the IAFM state. However, the converged total energy for the FM calculations in GGA+$U$ formalism is significantly higher (4927 meV/f.u.) than that found for IAFM couplings within GGA formalism. This suggests that the total energy in GGA+$U$ calculations may not represent the global minimum. Such scenario is often observed in GGA+$U$/LDA+$U$ calculations as well as documented in literature.[7,21–23] All these results indicate an IAFM ground state in this compound, consistent with the experimental results. Therefore, all the following calculations were carried out considering the intrachain antiferromagnetic coupling.

The calculated band gaps in the vicinity of $\epsilon_F$ for up-spin and down-spin density of states are shown in Fig. 4. It is evident from the figure that consideration of the electron correlation for both Ni $3d$ and Rh $4d$ electrons helps achieve the insulating phase. We have shown two types of results in the figure: (i) the dependence of the band gap as a function of $U_{dd}^{\mathrm{Ni}}$ for a fixed value of $U_{dd}^{\mathrm{Rh}}=3$ eV and (ii) band gap as a function of $U_{dd}^{\mathrm{Rh}}$ for a fixed value of $U_{dd}^{\mathrm{Ni}}=5.5$ eV. In the up-spin channel [see Fig. 4(a)], it is evident that an increase in $U_{dd}^{\mathrm{Ni}}$ does not lead to insulating phase until $U_{dd}^{\mathrm{Ni}}=4$ eV. An increase in $U_{dd}^{\mathrm{Ni}}$ above 4 eV provides an energy gap of about 0.12 eV. Interestingly, the band gap remains unchanged for further increase in $U_{dd}^{\mathrm{Ni}}$. On the other hand, the calculations as a function of $U_{dd}^{\mathrm{Rh}}$ for $U_{dd}^{\mathrm{Ni}}=5.5$ eV indicate gradual increase in band gap. Thus, the energy gap is essentially determined by $U_{dd}^{\mathrm{Rh}}$ when $U_{dd}^{\mathrm{Ni}}$ is kept large. Figure 4(a) suggests that the creation of insulating ground state requires $U_{dd}^{\mathrm{Rh}}$ to be at least 2.6 eV. Since the Coulomb repulsion strength depends inversely on the separation of the two electrons, the strength of on-site Coulomb interaction is sensitive to the radial extension of the wave functions. The present result of $U_{dd}^{\mathrm{Ni}}$, which is larger than $U_{dd}^{\mathrm{Rh}}$, is consistent with this behavior.

Calculations for the down-spin channel exhibit gradual increase in band gap with the increase in $U_{dd}$ for both Ni $3d$ and Rh $4d$ electrons. The magnitude of the gap in this case is always much higher ($>2$ eV) than that ($<1$ eV) observed for up-spin density of states. It is thus clear that various electronic properties of this compound will essentially be controlled by electronic density of states in the up-spin channel.

In order to investigate the character of the electronic states in the valence band, we show the calculated PDOS for

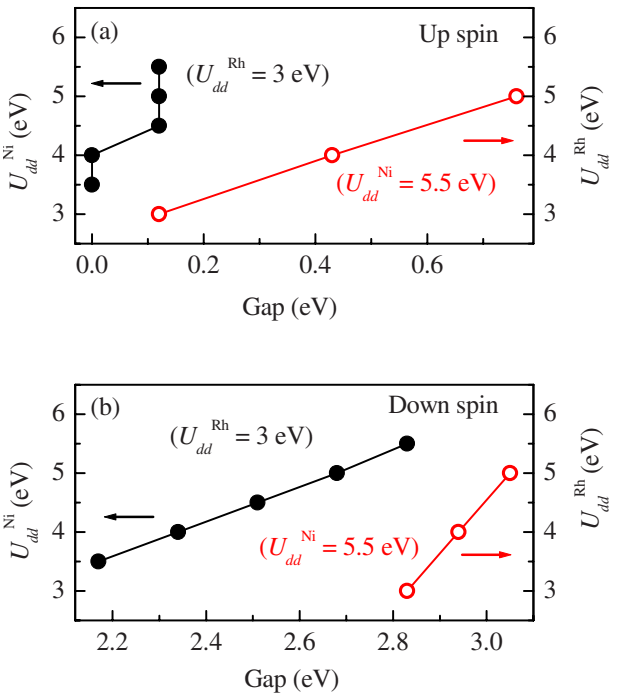


FIG. 4. (Color online) On-site Coulomb interaction among Ni $3d$ ($U_{dd}^{Ni}$) and Rh $4d$ ($U_{dd}^{Rh}$) electrons vs insulating gap for (a) up-spin and (b) down-spin channels. Two cases are considered: (i) $U_{dd}^{Rh}$ is fixed at 3 eV and $U_{dd}^{Ni}$ varied from 3.5 to 5.5 eV (solid circles), and (ii) $U_{dd}^{Ni}$ is fixed at 5.5 eV and $U_{dd}^{Rh}$ varied from 3 to 5 eV (open circles).

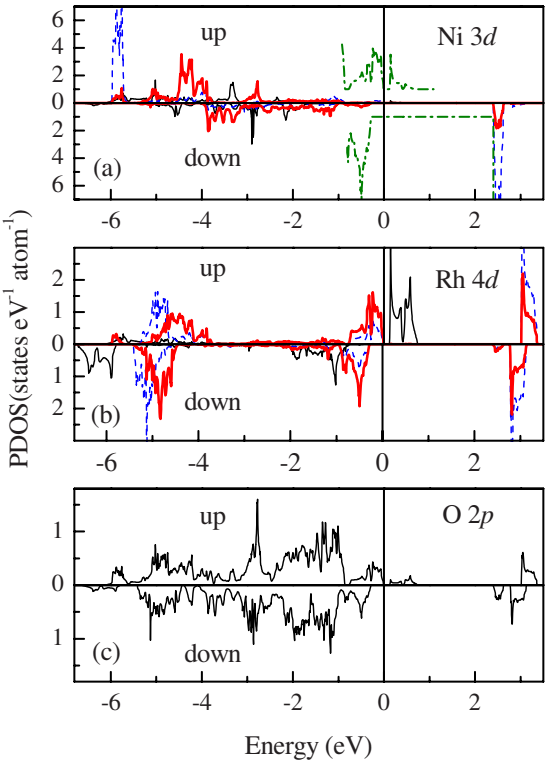


FIG. 5. (Color online) The PDOS corresponding to $d_{z^2}$ ($d_0$; thin solid lines), $d_{xz}+d_{yz}$ ($d_{\pm 1}$; dashed lines), and $d_{xy}+d_{x^2-y^2}$ ($d_{\pm 2}$; thick solid lines) orbitals for (a) Ni and (b) Rh, obtained from spin-polarized GGA+$U$ calculation ($U_{dd}^{Ni}$=5 eV and $U_{dd}^{Rh}$=3 eV) when intrachain Ni and Rh are antiferromagnetically coupled. (c) O $2p$ PDOS.

$U_{dd}^{Ni}$=5 eV and $U_{dd}^{Rh}$=3 eV in Fig. 5. All the bands are significantly modified due to the spectral weight transfer from $\epsilon_F$ to the energy region away from it. Ni $3d_{\pm 1}$ contributions exhibit significant band narrowing. The up-spin bands appear around −5.8 eV and the down-spin ones around 2.5 eV. The contributions from other Ni $3d$ orbitals appear between −2−−5 eV. Interestingly, the consideration of $U_{dd}^{Ni}$ leads to a significant increase in Ni $3d$ character at higher energies. Thus the O $2p$ contributions relative to Ni $3d$ become significantly high in the vicinity of the Fermi level.

Consideration of the on-site Coulomb interaction among Rh $4d$ electrons reveals large effect on the density-of-states distribution. In the GGA calculation, $d_0$ band was almost fully occupied, and there was a significant contribution of $d_{\pm 1}$ and $d_{\pm 2}$ orbitals within 0.28 eV of $\epsilon_F$ in the unoccupied up-spin channel, as evident from Fig. 3(b). This trend is reversed in GGA+$U$ calculations where the region within 0.75 eV above the $\epsilon_F$ is contributed by the electronic states having $d_0$ character. The electronic states below $\epsilon_F$ are contributed by $d_{\pm 1}$ and $d_{\pm 2}$ orbitals.

Despite the fact that the Ni $3d$ PDOS appear far away from $\epsilon_F$, it has finite contribution in the vicinity of $\epsilon_F$. This is evident in the rescaled Ni $3d$ PDOS (×15+1) shown in Fig. 5(a) by dot-dashed line. Interestingly, the energy distribution of these densities of state closely follows the distribution observed in Rh $4d$ and O $2p$ PDOS. This clearly manifests the effect of hybridization between Ni $3d$ and Rh $4d$ states via O $2p$ states. Most interestingly, the gap in the up-spin channel is much smaller than that found in down-spin channel. Thus, this system provides a unique example of a semiconductor where the electronic conduction is spin polarized. While half-metallic materials have long been investigated due to spin-polarized conduction of charge carriers in this system. This compound manifests properties that can be more useful in the semiconductor industry where spin based technology is envisaged.

Now, we discuss the manifestation of intrachain antiferromagnetic coupling and Coulomb correlation in the band structure along different high-symmetry directions of the Brillouin zone. The dispersion curves corresponding to different bands for FM, IAFM and IAFM with $U_{dd}^{Ni}$=5 eV and $U_{dd}^{Rh}$=3 eV for both the spin channels, are plotted in Fig. 6. The zero in the energy scale indicates $\epsilon_F$. In the ferromagnetic solution, the up-spin bands along $\Gamma M$ and $\Gamma A$ directions do not cross the Fermi level while the down-spin bands cross $\epsilon_F$ in all the directions, indicating half metallicity along these directions. The antiferromagnetic coupling among Ni and Rh in the chains leads to narrowing of the bands, and the up-spin bands cross the Fermi level in all the directions. On the other hand the down-spin bands in the vicinity of $\epsilon_F$ essentially appear below $\epsilon_F$. Again, the band crossing of the down-spin band is observed only along $K\Gamma$ direction, suggesting half metallicity in other directions.

Inclusion of the electron correlation among the $d$ electrons leads to significant change in the band structure. While there is a hard gap in both the spin channels consistent with the

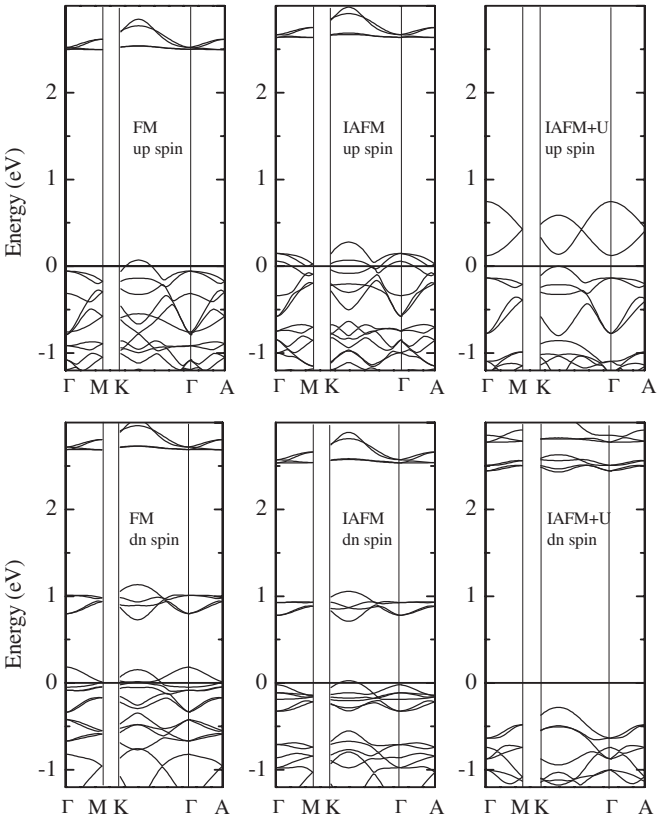


FIG. 6. Dispersion curves along different symmetry directions of the first Brillouin zone for both the spin channels. Fermi level is denoted by zero in the energy scale.

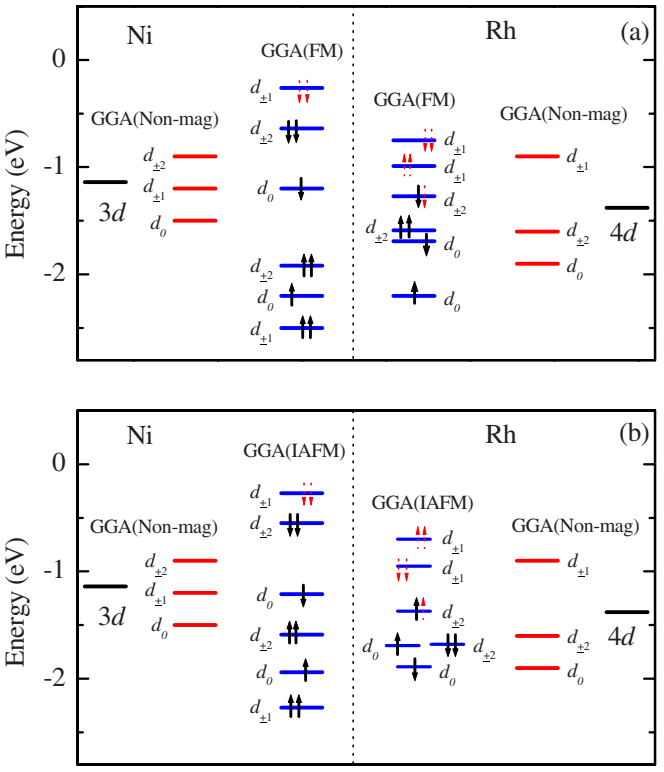


FIG. 7. (Color online) Schematic energy-level diagram of $d_0$, $d_{\pm 1}$, and $d_{\pm 2}$ orbitals for $Ni^{2+}$ and $Rh^{4+}$, obtained from (a) nonmagnetic (Nonmag) and FM calculations, and (b) Nonmag and IAFM calculations. Solid and dashed arrows indicate the occupied and unoccupied states, respectively.

transport behavior of this compound, the gap exhibits significant $k$ dependence. The gap at the high-symmetry point Γ is lower than that observed at $M$, $K$, or $A$ points. Interestingly, the dispersion of the bands close to $\epsilon_F$ appears to be larger than that observed in the uncorrelated case. This indicates that although electron correlation essentially tends to localize the electrons, the electronic states in the vicinity of the Fermi level are highly mobile.

The occupancies of different $d$ orbitals corresponding to Ni and Rh obtained from GGA+$U$ ($U_{dd}^{\mathrm{Ni}}$=5 and $U_{dd}^{\mathrm{Rh}}$=3 eV) calculation are shown in Table I. In up-spin channel, all the Ni 3$d$ orbitals are almost completely filled and in down-spin channel, only $d_{z^2}$ orbital is completely filled. The small deviations (~0.05) from the completely filled values can be attributed to the hybridization of Ni 3$d$ orbitals with the neighboring O 2$p$ orbitals. Total number of electrons in the Ni 3$d$ is found to be 7.91, which suggests that the valency of Ni is close to 2+.

TABLE I. The electron occupancies of $d_{z^2}$, $d_{xz}+d_{yz}$, and $d_{x^2-y^2}+d_{xy}$ orbitals for Ni and Rh obtained from spin-polarized GGA+$U$ calculation.

| | $d_{z^2}$ | $d_{xz}+d_{yz}$ | $d_{x^2-y^2}+d_{xy}$ | Total |
|---|---|---|---|---|
| Ni-up | 0.94 | 1.96 | 1.9 | 4.8 |
| Ni-down | 0.95 | 0.56 | 1.6 | 3.11 |
| Rh-up | 0.21 | 1.0 | 1.3 | 2.51 |
| Rh-down | 0.82 | 1.04 | 1.32 | 3.18 |

In the case of Rh 4$d$ orbitals, both the spin channels are partially occupied. Our calculations exhibit 5.69 electrons in the Rh 4$d$ orbitals. If we consider O in 2− and Sr in 2+ states, then charge neutrality condition demands Rh to be in 4+ state, which corresponds to five electrons in the 4$d$ orbitals. The extra 0.69 electrons can be attributed to strong hybridization of Rh 4$d$ orbitals with the neighboring O 2$p$ orbitals.

The calculated magnetic moments for Ni and Rh in the IAFM configuration are $1.69\mu_B$ and $-0.68\mu_B$, respectively, with almost negligible contribution from oxygen ($0.01\mu_B$). The total magnetic moments per formula unit, including the contribution of $-0.07\mu_B$ from the interstitial region, is found to be about $1\mu_B$, consistent with the experimental results.[6]

In order to provide a qualitative understanding of the intrachain antiferromagnetic interaction between Ni and Rh moments, we show the schematic of crystal-field split energy levels for both Ni and Rh in Fig. 7. These energy levels were estimated by the centers of gravity of $d_0$, $d_{\pm 1}$, and $d_{\pm 2}$ PDOS obtained from nonmagnetic (DOS and PDOS are not shown in the manuscript), FM (Fig. 2), and IAFM (Fig. 3) GGA calculations.[24] The energy separations (crystal-field splitting) of Ni $d_0$ and $d_{\pm 1}$, and $d_{\pm 1}$ and $d_{\pm 2}$ are found to be similar and is about 0.3 eV. The energy separations of Rh $d_0$ and $d_{\pm 2}$ and $d_{\pm 2}$ and $d_{\pm 1}$ are about 0.3 and 0.7 eV, respectively.

In the magnetic case, the exchange coupling leads to splitting of the $d_0$, $d_{\pm 1}$, and $d_{\pm 2}$ levels to their up- and down-spin

counterparts. Thus, the exchange coupling strength $J$ may be estimated by the separation of the center of gravity of the up- and down-spin bands. In the FM case, $J$ among Ni $3d$ states are about 1, 2.24, and 1.28 eV, and that among Rh $d$ states are found to be about 0.51, 0.24, and 0.32 eV, respectively. In the IAFM case, $J$ corresponding to Ni $d$ states reduce to 0.73, 2, and 1.04 eV, respectively. The exchange energies of Rh $d_{\pm 1}$ and $d_{\pm 2}$ electrons remain almost the same as in the FM case, and that for $d_0$ electrons reduces to 0.2 eV.

The occupancy of various energy levels is shown by solid arrows and the unoccupied levels by dashed arrows in the figure. In the ionic limit, eight electrons in $Ni^{2+}$ will occupy all the lower five levels and $d_{\pm 1}$ down-spin level will be empty. In the FM state [see Fig. 7(a)], five electrons in $Rh^{4+}$ will occupy such that the $d_{\pm 2}$ down-spin level will be half filled. In the case of IAFM state [see Fig. 7(b)], the $d_{\pm 2}$ up-spin level will be half filled. It is evident from the figure that in the FM case, only down-spin electrons can transfer from Ni to Rh sites and vice versa. But in the IAFM case, both the up- and down-spin electrons can transfer among these sites, and the number of unoccupied levels available for such transfers is larger than those in FM state. Clearly the cost of energy for such electron transfers is lower in the case of IAFM configuration. This suggests IAFM state as a favorable ground-state configuration compared to the FM state.[25]

## IV. CONCLUSIONS

In conclusion, we studied the electronic and magnetic properties of $Sr_3NiRhO_6$ using *ab initio* spin-polarized band-structure calculations within GGA and GGA+$U$. The calculations for intrachain antiferromagnetic coupling exhibit the lowest energy. The magnetic moments of Ni and Rh ions were found to be $\sim 1.7\mu_B$ and $-0.7\mu_B$, respectively, with a total moment of about $1\mu_B$. All these results corresponding to the magnetic phase provide a remarkable representation of the experimental results.

The insulating phase observed in transport measurements could not be captured within GGA, suggesting the importance of electron correlation. GGA+$U$ calculations reveal that the critical values of Coulomb correlation strength to open up the insulating gap are $\sim 4.5$ and $\sim 2.5$ eV for Ni $3d$ and Rh $4d$ electrons, respectively. The inclusion of electron correlation leads to significant change in character of the energy bands. The feature close to $\epsilon_F$ exhibits enhancement of O $2p$ character while the $d$ character enhances at higher energies. Interestingly, the band gap in up-spin channel is found to be significantly small ($\sim 0.12$ eV) compared to that observed ($>2$ eV) in the down-spin channel, indicating possibilities of spin-polarized conduction in the semiconducting phase.

## ACKNOWLEDGMENTS

The authors acknowledge E. V. Sampathkumaran, TIFR, India for drawing our attention toward this compound and useful discussions.

*kbmaiti@tifr.res.in

[1] S. Niitaka, H. Kageyama, M. Kato, K. Yoshimura, and K. Kosuge, J. Solid State Chem. **146**, 137 (1999).
[2] E. V. Sampathkumaran and A. Niazi, Phys. Rev. B **65**, 180401(R) (2002).
[3] D. Flahaut, S. Hébert, A. Maignan, V. Hardy, C. Martin, M. Hervieu, M. Costes, B. Raquet, and J. M. Broto, Eur. Phys. J. B **35**, 317 (2003).
[4] S. Agrestini, C. Mazzoli, A. Bombardi, and M. R. Lees, Phys. Rev. B **77**, 140403(R) (2008).
[5] S. Niitaka, K. Yoshimura, K. Kosuge, M. Nishi, and K. Kakurai, Phys. Rev. Lett. **87**, 177202 (2001).
[6] N. Mohapatra, K. K. Iyer, S. Rayaprol, and E. V. Sampathkumaran, Phys. Rev. B **75**, 214422 (2007).
[7] H. Wu, Z. Hu, D. I. Khomskii, and L. H. Tjeng, Phys. Rev. B **75**, 245118 (2007).
[8] K. E. Stitzer, W. H. Henley, J. B. Claridge, H.-C. zur Loye, and R. C. Layland, J. Solid State Chem. **164**, 220 (2002).
[9] K. Sengupta, S. Rayaprol, K. K. Iyer, and E. V. Sampathkumaran, Phys. Rev. B **68**, 012411 (2003).
[10] M.-H. Whangbo, D. Dai, H.-J. Koo, and S. Jobic, Solid State Commun. **125**, 413 (2003).
[11] R. Vidya, P. Ravindran, H. Fjellvåg, A. Kjekshus, and O. Eriksson, Phys. Rev. Lett. **91**, 186404 (2003).
[12] E. V. Sampathkumaran, N. Fujiwara, S. Rayaprol, P. K. Madhu, and Y. Uwatoko, Phys. Rev. B **70**, 014437 (2004).
[13] R. Frésard, C. Laschinger, T. Kopp, and V. Eyert, Phys. Rev. B **69**, 140405(R) (2004).
[14] H. Wu, M. W. Haverkort, Z. Hu, D. I. Khomskii, and L. H. Tjeng, Phys. Rev. Lett. **95**, 186401 (2005).
[15] K. Takubo, T. Mizokawa, S. Hirata, J.-Y. Son, A. Fujimori, D. Topwal, D. D. Sarma, S. Rayaprol, and E.-V. Sampathkumaran, Phys. Rev. B **71**, 073406 (2005).
[16] J. Sugiyama, H. Nozaki, Y. Ikedo, P. L. Russo, K. Mukai, D. Andreica, A. Amato, T. Takami, and H. Ikuta, Phys. Rev. B **77**, 092409 (2008).
[17] P. Blaha, K. Schwarz, G. K. H. Madsen, D. Kvasnicka, and J. Luitz, *WIEN2k, An Augmented Plane Wave Plus Local Orbitals Program for Calculating Crystal Properties* (Karlheinz Schwarz, Technische Universität Wien, Austria, 2001).
[18] Z. Wu and R. E. Cohen, Phys. Rev. B **73**, 235116 (2006).
[19] V. I. Anisimov, I. V. Solovyev, M. A. Korotin, M. T. Czyżyk, and G. A. Sawatzky, Phys. Rev. B **48**, 16929 (1993).
[20] V. I. Anisimov, F. Aryasetiawan, and A. I. Lichtenstein, J. Phys.: Condens. Matter **9**, 767 (1997).
[21] M. A. Korotin, S. Yu. Ezhov, I. V. Solovyev, V. I. Anisimov, D. I. Khomskii, and G. A. Sawatzky, Phys. Rev. B **54**, 5309 (1996).
[22] S. K. Pandey, A. Kumar, S. Patil, V. R. R. Medicherla, R. S. Singh, K. Maiti, D. Prabhakaran, A. T. Boothroyd, and A. V. Pimpale, Phys. Rev. B **77**, 045123 (2008).
[23] S. K. Pandey, S. Patil, V. R. R. Medicherla, R. S. Singh, and K. Maiti, Phys. Rev. B **77**, 115137 (2008).
[24] I. A. Nekrasov, S. V. Streltsov, M. A. Korotin, and V. I. Anisimov, Phys. Rev. B **68**, 235113 (2003).
[25] J. B. Goodenough, *Magnetism and the Chemical Bond* (Interscience, New York, 1963).